MRS Advances © 2017 Materials Research Society
DOI: 10.1557/adv.2017.481

Modeling and simulation of microstructural evolution in Zr based Bulk Metallic Glass Matrix Composites during solidification

Muhammad Musaddique Ali Rafique[1], Dong Qiu[1], Mark Easton[1]

[1]School of Engineering [Aerospace, Mechanical and Manufacturing Engineering], RMIT University, Queensbury Street, Carlton, 3053 VIC, AUSTRALIA

ABSTRACT

Bulk metallic glass and their composites are unique new materials which have superior mechanical and structural properties as compared to existing conventional materials. Owing to this, they are potential candidates for tomorrow's structural applications. However, they suffer from disadvantages of poor ductility and little or no toughness which render them brittle and they manifest catastrophic failure on the application of force. Their behavior is dubious and requires extensive experimentation to draw conclusive results. In present study, an effort has been made to overcome this pitfall by simulation. A quantitative mathematical model based on KGT theory has been developed to describe nucleation and growth of second phase dendrites from melt in glassy matrix during solidification. It yields information about numerical parameters necessary to understand the behaviour of each individual element in multicomponent sluggish slurry and their effect on final microstructural evolution. Model is programmed and simulated in MATLAB®. Its validation is done by comparison with identical curves reported in literature previously for similar alloys. Results indicate that the effect of incorporating all heat transfer coefficients at macroscopic level and diffusion coefficients at microscopic level play a vital role in refining the model and bringing it closer to actual experimental observations. Two types of hypo and eutectic systems namely $Zr_{65}Cu_{15}Al_{10}Ni_{10}$ and $Zr_{47.5}Cu_{45.5}Al_5Co_2$ respectively were studied. Simulation results were found to be in good agreement with prior simulated and experimental values.

INTRODUCTION

Bulk Metallic Glasses [1] have emerged [2] as competitive structural engineering material [3] during last two decades and have attracted the attention of several major research groups [4-18] around the word to further probe into the science and engineering behind their formation [19], microstructural evolution [20], property development and structure – property relationship [21, 22]. Main areas of focus have been investigation of evolution of mechanical properties in these materials as despite their high hardness and very high elastic strain limit, they do not exhibit any tensile ductility and fail catastrophically [23, 24] under tensile and impact loading. This happens due to rapid movement of shear bands [25-32] in the volume of materials by virtue of which material does not exhibit any yielding. Infact, they exhibit strain softening rather than strain hardening upon deformation in tensile loading [33-35]. These behaviors render them useless in practical structural engineering applications [36, 37]. In addition to that, they are limited by the size in which 100% monolithic glassy structure can be achieved [38]. Chemical compositions in which it is possible are rather limited and difficult to process into useful shapes due to their multicomponent nature which make the material thick / slurry like and sluggish during processing. Various mechanisms have been proposed to overcome these drawbacks. Some of them include; increasing the number and complexity of shear bands by allowing their multiplicity due to (a) self-interaction or (b) at sites of foreign particles purposefully introduced

to create sites of multiplication of shear bands [39]. On the other hand there have been efforts to study evolution of phases during liquid to solid transformation of these materials by their investigation in synchrotron light [40, 41] using container less levitation solidification techniques. Efforts have also been made to study same phenomena in micro and zero gravity conditions on board International Space Station (ISS). Various theories such as Liquid – Liquid Transition (LLT) [42], Phase separation prior liquid – to – solid transformation [43] have been proposed to explain their microstructural evolution but still, there is dearth of knowledge about their exact mechanisms of formation and microstructural evolution [44]. With experimental methodologies, efforts have also been focused to utilize well established solidification theories [45-47] to investigate and predict microstructural evolution during solidification using advanced multi scale and parallel modeling and simulation strategies. Various algorithms [48-51] have been proposed which are associated with development of microstructure in multicomponent alloys [52]. In this study, an effort has been made to further extend this approach and use deterministic methods to calculate numerical parameters necessary to understand microstructural evolution of ductile phase in BMGMCs during solidification. An indigenous, in house model have been developed using famous KGT [46] and Rappaz [45] model to predict microstructural evolution during solidification of Zr based BMGMC. This is first effort of its kind which utilizes strengths of both approaches to formulate a comprehensive model for the prediction of microstructure primarily explaining dendrite tip temperature and dendrite tip radius as a function of growth rate / dendrite tip velocity.

THEORY (MATHEMATICAL MODEL)

Durig this study only deterministic apporach is adopted to arrive at numeical quantitative parameters necessary to describe solidification and microstructre evolution during initial stage of alloy cooling. Further visual obervation of real time microstructure may be described by coupling [47, 53, 54] of present model with well established probablistic models [45, 55, 56] based on cellular automaton theory [57, 58]. For present case, considering a free dendrite tip of parabolic shape, KGT model [46] is taken to be responsible for microstructural evolution. Its basic assumptions are following;

1. The solute field around the dendrite tip is given by Ivantsov solution.
2. The dendrite tip grows at marginal stability limit.
3. The diffusion coefficient d, is (tip) temperature dependent.
4. The segregation / partitition coefficient, k, takes into account solute trapping; i-e, k is (dendrite tip) velocity dependent.
5. Initial partition coefficient (k_o) is temperature dependent and binary alloy (Zr – Cu) is assumed to behave as multicomponent alloy.
6. The undercooling of tip (ΔT) is the sum of solute undercooling and the curvature undercooling.
7. The effect of convection is ignored.

In present study, hoewever, a further practical approach is adopted which takes into account the calculation of supersaturations of individual consitituents / components in alloy which rules out that their diffusion fields superimpose and binary alloy system is assumed to behave as ternary or

multicomponent system (BMGMC). This is a contradiction to assumption 5 above in basic KGT model – a unique approach adopted here to explain microstructural evolution in detail.

There are three main velocities of interest here (Figure 1 (a – c)) when a beam of high energy (electron or laser) travels on surface of specimen in additive manufacturing setup (Figure 2)

1) Moving heat source velocity (V_b), 2) Solidification front velocity (V_s) and 3) Dendrite tip velocity (V_{hkl})

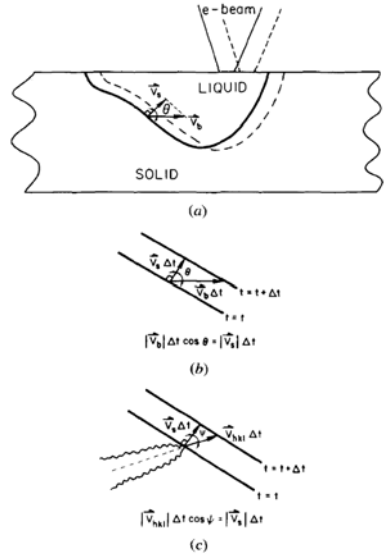

Figure 1 (a – c): Schematic showing relationship between different velocity components (reprinted with permission from Springer) [49]

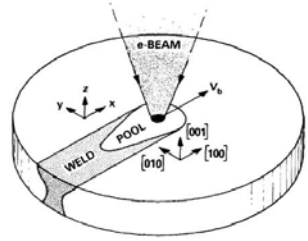

Figure 2: Schematic of melt pool formation in additive manufacturing (EBM) and velocity of heat source (reprinted with permission from Springer) [49]

Model consists of three main parts and separate mathematical expression is developed for each segment.

Nucleation

This is based on Oldfield theory of heterogeneous nucleation which describes a relationship between undercooling (ΔT) and grain density at each segment of interest (bulk liquid, mold wall and potent nuclei) in terms of Gaussian distribution. Two most important parameters namely, maximum nucleation density (n_{max}) and Grain density ($n(\Delta T)$) are sought after to be determined. Maximum nucleation density may be obtained by integral of nucleation distribution from zero undercooling to infinite undercooling.

$$n_{max_i} = \int_0^{\infty} \frac{dn}{d\Delta T'} \Delta T' \qquad [1]$$

Similarly, grain density is given by following equation

$$n(\Delta T) = \int_0^{\Delta T} \frac{n_{max}}{\Delta T_\sigma \sqrt{2\pi}} exp\left[-\frac{1}{2}\left(\frac{\Delta T' - \Delta T_N}{\Delta T_\sigma}\right)\right] d\Delta T' \qquad [2]$$

where ΔT_n and ΔT_σ are mean undercooling and standard deviation of grain density distribution respectively.

With this, probability of happening of one event (nucleation) is given by nucleation probability (p_v) as described by Prof. Rappaz in his famous article [45].

$$p_v \geq r \qquad [3]$$

i-e if at any instant of time t, p_v exceeds r, nucleation will occur. $p_v = \delta n_v . V_{CA}$ where δn_v = grain density increase and V_{CA} = one cell volume (measure by noting all dimensions of cell assuming it to have square shape) (Figure 3(a)). A change in state index of a cell represents its growth as depicted by cells in Figure 3(b). Typically cell dimensions are in nanometers while typical number of cells reported in previous calculations are 30,000 [51]

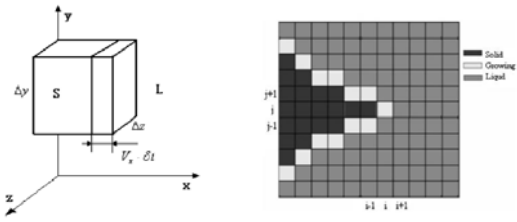

(a) (b)

Figure 3: (a) Schematic of growth in one cell (b) Schematic diagram of movement of dendrite tip in a grid of cells represented by change of state index of each cell (reprinted with permission from Taylor and Francis Group) [47]

Dendrite growth orientation

Second part of the model deals with determining dendrite growth orientation i-e the direction in which some dendrites preferably grow faster and longer as compared to others due to balance between geometrical and kinetic variables. This also highlights and points towards grain competition and selection mechanisms. Two important parameters are considered for assigning and determining grain orientation. a) Growth of first grain as a result of heterogeneous nucleation at mold wall or potent nuclei and b) Location of further subsequent new grain(s) and

their crystallographic orientation. For example, for cubic metals, the preferential growth directions of dendrites are given by direction of easy heat flow which is along (100) crystallographic direction / orientation. During early stage of solidification, a nucleus grows at the surface of mold or potent nuclei in the form of hemispherical surface. This surface becomes unstable and then dendritic after a certain incubation time and growth occurs with main trunk and arms coinciding with (100) crystallographic direction. The location of new grains is assumed to be governed by random process. This specific orientation is described to be governed by three Euler angles θ, φ and ψ irrespective of grain nucleated at the surface of mold, potent nuclei or bulk liquid. First two angles describes the growth and orientation of main [001] trunk while third angle ψ describes the orientation of [100] and [010] secondary branches. A schematic showing the arrangement is shown in figure below (Figure 4)

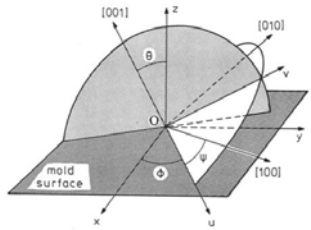

Figure 4: Schematic of crystallographic orientation of new nucleated grain as defined by three Euler Angles, θ, φ and ψ (reprinted with permission from Springer) [51]

The probability dp(θ, φ, ψ) that a newly nucleated grain has its main trunk orientation in the range [$\theta, \theta + d\theta$] and [$\varphi, \varphi + d\varphi$] and one of its set of secondary branches within the orientation [$\psi, \psi + d\psi$] is given by [51]

$$dp(\theta, \varphi, \psi) = A \,.\, \sin\theta \,.\, d\theta \,.\, d\varphi \,.\, d\psi \qquad [4]$$

where A = constant which takes into account the fourfold symmetry of the dendrite along its trunk axis and the possible permutations of the (100) directions.
In general, dendrite growth direction of grain nucleated at the mold surface determines the time during which grain can survive competitive growth of its neighbors.

Grain growth / Growth kinetics / Dendrite stability theory

This section concerns kinetics associated with growth of already formed grains in bulk liquid, mold surface and potent nuclei. A unique feature adopted here constitutes the determination of supersaturation of individual elements in multicomponent alloy (BMGMC) systems. This approach originates from the fact that in contrast to conventional castings in which undercooling related with thermal diffusion, attachment kinetics and curvature is small, in multicomponent systems basic KGT model must be used with certain modifications which not only accounts for superimposition of solute fields around each dendrite tip but also incorporate determination of supersaturation for each individual component (Zr, Cu, Ni, Al and Co) of alloy system. This supersaturation Ω_i is a function of Peclet number, Pe_i

$$\Omega_i = I_v(Pe_i) \qquad [5]$$
$$Pe_i = I_v(Pe_i) \qquad [6]$$

$$Pe_i = \frac{R.V}{2.D_i} \quad [7]$$

Putting in [5]

$$\Omega_i = I_v(\frac{R.V}{2.D_i}) \quad [8]$$

$$\Omega_i = P_e\, e^{P_e} E_1(P_e) = P_e\, e^{P_e} \int_{P_e}^{\infty} \frac{e^{-u}}{u} du \quad [9]$$

$$\Omega_i = \frac{R.V}{2.D_i} e^{\frac{R.V}{2.D_i}} E_1(P_e) = \frac{R.V}{2.D_i}\, e^{\frac{R.V}{2.D_i}} \int_{\frac{R.V}{2.D_i}}^{\infty} \frac{e^{-u}}{u} du \quad [10]$$

but

$$\Omega_i = \frac{c_i^* - c_{o,i}}{c_i^*(1-k_i)} \quad [11]$$

where

c_i^*= concentration of constituent i in liquid at dendrite tip (to be found), $c_{o,i}$= initial concentration of constituent i, k_i= partition coefficient for this constituent i (velocity dependent)

Comparing [10] and [11]

$$\frac{c_i^* - c_{o,i}}{c_i^*(1-k_i)} = \frac{R.V}{2.D_i}\, e^{\frac{R.V}{2.D_i}} \int_{\frac{R.V}{2.D_i}}^{\infty} \frac{e^{-u}}{u} du \quad [12]$$

However,

$$c_i^* = \frac{c_{o,i}}{1-(1-k_i)(I_v(Pe_i))} \quad [13]$$

$$k_i = \frac{k_o + (\frac{a_o V}{D_i})}{1 + (\frac{a_o V}{D_i})} \quad [14]$$

where

a_o = length scale related to interatomic distance and is estimated to be between 0.5 – 5 nm and

$$D_i = D_o e^{\left(-Q/R_g.T^*\right)} \quad [15]$$

where

D_o= Proportionality constant, Q = Activation energy, R_g = Gas constant, T* = Tip temperature calculated by iterative method (described below) [50]

In a linearized phase diagram

$$T^* = T_L + \sum_{i=1}^{2} m_i\left(c_i^* - c_{o,i}\right) - \frac{2\Gamma}{R} \quad [16]$$

where

m_i = slope of liquidus surface with respect to constituent *i*

$$m_i = \frac{\partial T_L}{\partial c_i} \quad [17]$$

T_L = Liquidus temperature for initial alloy composition, Γ = Gibbs – Thomson coefficient, $\frac{2\Gamma}{R} \approx$ 0 (negligible) (under normal solidification conditions), $\frac{2\Gamma}{R} = 1$ (under rapid solidification conditions)

Another term can be coined from linearized phase diagram known as fictitious melting point of pure constituent [50].

$$T_m{}' = T_L - \sum_{i=1}^{2} m_i c_{o,i} \qquad [18]$$

Using eq. (13) and (18), eq. (16) becomes

$$T^* = T_m{}' + \sum_{i=1}^{2} \frac{m_i c_{o,i}}{1-(1-k_i)(I_v(P_{ei}))} - \frac{2\Gamma}{R} \qquad [19]$$

where

R = Dendrite tip radius, V = Dendrite tip velocity

This model is iterative model which is based on assigning final values to original value generating loop whose explanation will be given in next section. 100 iterative cycles are used to generate homogeneous and normalized data. In general while writing the program, reading it and executing it, Ω depends on $I_v(Pe_i)$ and c_i^*, c_i^*depends on k_i and $I_v(Pe_i)$, k_i depends on D_i, D_i depends on Tip temperature and finally, Tip temperature depends on c_i^*

Thus a loop is generated which accounts for "to and fro" motion of information and iterative handling of data. This is the essence of generation of refined outputs and results.

Finally, total undercooling (ΔT) is related to supersaturation (Ω) by [51]

$$\Delta T_i = m_i.c_{o,i}.\left[1 - \frac{1}{1-\Omega_i.(1-k_i)}\right] \qquad (20)$$

The criteria used to specify radius of dendrite tip (R) is assumed to be given by marginal stability wavelength of planar wave front (as given in Mullins and Sekerka [59], Langer and Mueller – Krumbhaar [60], KGT [46] and BLL [61] models)

Accordingly, one has for a ternary system

$$R = 2\pi \left(\frac{\Gamma}{\sum_{i=1}^{2} m_i G_{c,i} \varepsilon_c(P_{ei}) - G}\right)^{1/2} \qquad (21)$$

where

$G_{c,i}$ = solute gradient of constituent *i* in the liquid near tip which can be written as

$$G_{c,i} = -\frac{v}{D_i} C_i^*(1-k_i) \qquad (22)$$

G = Average thermal gradient near tip and $\varepsilon_c(P_{ei}) = f(P_{ei}) = 1$ (low speed / low P_{ei})

Putting values of $P_{ei} = \frac{R.V}{2.D_i}$ and eq. (22) in eq. (21) [50]

$$\frac{4\pi^2\Gamma}{R^2} + \frac{2}{R}\sum_{i=1}^{2} \frac{P_{ei} m_i C_{o,i}(1-k_i)\xi_c(P_{ei})}{[1-(1-k_i)\mathrm{Iv}(P_{ei})]} + G = 0 \qquad (23)$$

where

Γ = Gibbs – Thomson coefficient, m_i = the slope of liquidus, ξ_c = a function of the Peclet number and segregation coefficient, G = Thermal gradient

SIMULATION USING OBJECT ORIENTED PROGRAMMING (OOP)

A computer program was written in MATLAB®. Instead of fixing the Peclet number as was done in previous approaches [50], this program account for changing Peclet number with the change of each state value of system. Furthermore, the program is based on transient transport processes and values are incorporated into original values using 'for' loop and are assigned to their initial values using iterative approach. This helps in improving the efficiency of program and generation of fine mesh less results. Program asks for initial values and upon assigning initial values to dynamic variables, it generates first set of data which is repeated and assigned back to original variable to generate a loop. This process is repeated 100 times based on the number of iterations assigned in loop. It also takes into account temperature dependent diffusion coefficient and velocity dependent partition / segregation coefficient in accordance with KGT model [46]. A correlation for the use of thermophysical data for major alloying elements of BMGMC systems was developed based on their presence in same reactive group (transition metals) in periodic table and nearest possible commonly studied element (Cr) [50] was chosen for generation of first set of data. Based on this, the parameters used in calculations are listed in Table 1. The thermal gradient (G) which is a function of additive manufacturing (AM) condition is taken as free number and only one value (100 K / mm) is used for calculations. A unique feature of program is it can work for; and be tailored according to the need of any material (alloy) and manufacturing process (additive manufacturing). Data on thermophysical properties of metals and alloys (especially exotic materials) as they change with the change of time and temperature is scarce and more efforts are needed in this front.

Table 1: Parameters used in the calculations of dendritic growth for Zr based BMGMCs

Sr. No.	Parameter	Description	Value
1	T_L	Liquidus temperature	2128 K
2	C_{oZr}	Initial concentration of Zr in alloy	0.65 wt %
3	R_i	Initial value of tip radius	0.001 mm
4	V_i	Initial value of dendrite tip velocity	2 mm / sec
5	D_o	Proportionality constant	0.492 mm^2 / sec
6	a_o	Length scale related to interatomic distance	0.000005 mm
7	Q	Activation energy for diffusion	67700 $J.mol^{-1}$
8	Γ	Gibbs Thomson Coefficient	1.90 x 10^{-4} (K mm)
9	R_g	Gas Constant	8.314 ($J.mol^{-1}.K^{-1}$)
10	G	Thermal Gradient	100 K / mm
11	H_f	Heat of fusion	21000 ($J.mol^{-1}$)
12	c	Constant related with unit thermal undercooling θ_t	1

EXPERIMENTAL

BMGMC samples were casted in two ways. Firstly, they are made in form of wedge using vacuum suction casting system in lab scale Vacuum Arc Melting (VAM) button furnace at CSIRO – Manufacturing. The process consists of carefully calculating raw material based on weight percentage of each element in the alloy system. These powders / granules / chucks are subsequently mixed using hand spatulas to a homogeneity observable by naked eye. For their positioning, handling and control inside enclosed chamber of VAM, they are wrapped in an

aluminum foil which not only protects the powders but also serve to fulfill the requirement of alloying element in sufficient quantity in original mix. This Aluminum foil wrapped toffee is placed in horizontal slot in the Copper hearth of water cooled furnace at appropriate time after which, it is melted to get solid chuck / button for subsequent research. During second approach, casted wedge samples were subjected to laser solid forming (LSF) [62] in Additive Manufacturing Setup. Model theory was developed and tailored to describe microstructure evolution during both processes.

RESULTS AND DISCUSSION

Model works by explaining dendritic growth in cast alloys during solidification by manipulating physical process parameters with the change of heat and mass transfer coefficients. Its unique feature is it explains the behavior of multicomponent alloys in terms of transient state variables. An effort is made to keep constant values to a minimum to get real picture of actual physical processes. Boundary conditions of solidification phenomena are kept open which makes model more rigorous and robust and it is possible to apply this for various alloys systems under various conditions. Following results and graphs have been generated after writing script of solidification code and running it in MATLAB®.

Effect of heat dissipation on dendrite tip velocity

Figure 5 is the plot of evolution of solutal Peclet number of different elements of BMGMC system against their dendrite tip growth velocities. It shows the transport behavior of individual elements with the change and evolution of state variables. It is clearly evident that highest growth velocity has been attained by Zirconium with very little heat loss from system to surrounding. One of the reasons this happens is due to higher atomic weight and size of

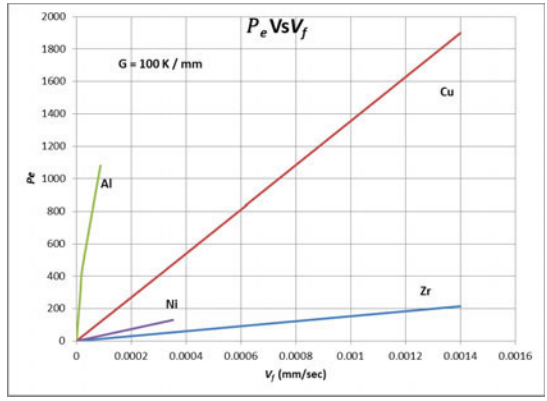

Figure 5: Plot of solutal Peclet number Vs dendrite tip velocity for individual elements of BMGMC system

Zirconium atoms by virtue of which they can travel higher and longer in slurry like thick multicomponent system with causing very little or no interaction with surrounding material / elements. That is they; owing to their large size attain a more favorable position and orientation while navigating through thick fluid which consists of elements of various size ranges and

undergoing rapid heat loss and due to solidification. Thermal conductivity of Zirconium is also not very high which suggest that very little heat loss will occur as a result of Zirconium, its presence and movement through fluid. Overall large atomic weight remains as the major factor for its increased dendrite tip velocity through thick slurry. A small effect of gravity also contributes towards this overall effect (not considered in detail here). Second element of interest in this multicomponent system is Ni, which is not been able to attain enough velocity in growing dendrite tip due to its lower atomic weight. Thus it remains ineffective in creating shear zone around it which can allow it to penetrate and gain speed in thick slurry around it. It also does not have very high thermal conductivity thus not a lot of heat gets dissipated because of it to surrounding and again it reflects its inability to create low viscosity zone around it which may facilitate it to gain high speeds. A drastically high speed and very high Peclet number over a range is depicted by Copper. This was not astonishing, as it is the element of highest thermal conductivity with an intermediate position with respect to its atomic weight in periodic table of elements. These both features; specially high thermal conductivity gives it an edge to create a region of very high heat dissipation around it facilitating its motion at a high speed over a range of Peclet number in a thick slurry of multicomponent alloy systems. The atomic size and configuration of copper is also favorable for attaining this high speed. Thus for this thermal gradient, it remains as the most important element contributing towards overall speed / dendrite tip growth velocity of system. The last element is Aluminum, which despite of its high thermal conductivity does not attain very speed. This happens because; the atomic size and weight of aluminum is not very high which does not help it to gain high velocity in the thick slurry of multicomponent systems at tip of dendrite. Also, as the heat keeps on getting dissipated from its surrounding and it has relatively low atomic weight as compared to others, it does not attain high speed and gets stuck in its own region. This reasoning is based on atomic size, weight, electronic configuration and thermal conductivity of individual elements. However, no data exists about actual dendrite growth velocity of this complex BMGMC system and further experimental research to measure this is needed.

Effect of tip temperature on dendrite tip velocity

Below graph (Figure 6) shows relationship between dendrite tip velocity as a function of dendrite tip temperature for Zirconium only in the systems considering it to be major alloying element. Graph shows three different regions which are distinctive of velocity evolution of Zr in the system as temperature change. There is a sharp increase in T_{tip} at slow V_f because dendrites are equiaxed in nature and due to their rapid mechanical interaction with each other a lot of heat is accumulated in small area. This is more evident in multicomponent alloys. Here, since only Zirconium is under consideration, so the large atomic size and weight of Zr also contribute towards increase of this value. This is early / initial stage of solidification. Another reason for this is there is planar wave front during initial stages which does not allow the development of high surface area i-e surface area / volume ratio remain low and not a lot of heat gets dissipated. This is also shown in previous works by Rappaz et. al. [50] but as equiaxed to columnar transition (ECT) stage reaches, a stability region evolves. It happens due to very nice delicate balance between heat loss at dendrite tip and growth velocity of propagating solidification front. After that, again drop in T_{tip} with increase in velocity is observed. This happens as Zr dendrite gain speed; they start creating regions of very high surface / volume ratio around them in the body of melt and at the tip of advancing dendrite. In other words faster moving dendrites become source of high heat dissipation. Owing to this, temperature comes down

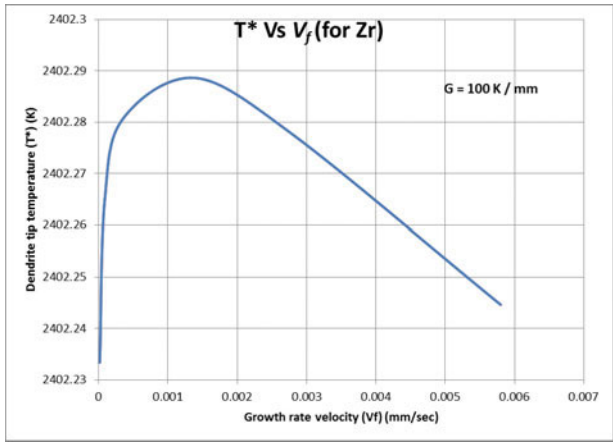

Figure 6: Plot of dendrite tip temperature Vs dendrite tip velocity for Zr in BMGMC system.

Effect of ξ (a function of P_{el}) on P_{el}

Below graph (Figure 7) is representation of ξ with respect to Peclet number. It briefly shows that ξ (which is a function of P_e) shows almost decreasing linear relationship with the increase of rate of heat transfer from system to surrounding for all major alloying elements of hypoeutectic system at a fixed thermal gradient. It shows the effectivity of heat transfer process for BMGMC and gives measure that dissipation was proper and homogenous. The curves are generated by plotting solution of present model by the use of indigenous MATLAB code incorporating different transient thermo-physical data of each individual alloy system from literature [63-68]. Simulation results are in nice agreement with previously reported behavior of elements in alloy systems [61]. It clearly indicates that ξ value finally turns to zero for all elements generating a nice synergy between simulation and experimental observations in high speed additive manufacturing processes.

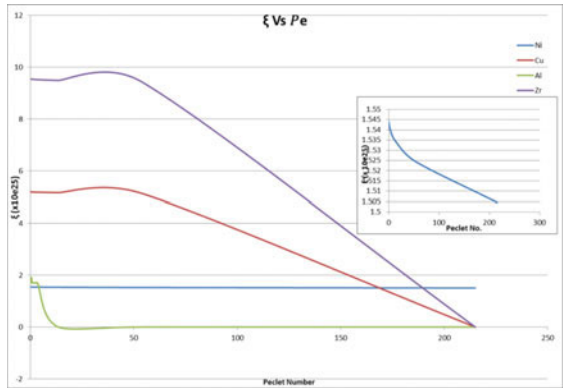

Figure 7: Plot of ξ Vs Peclet number for various elements in BMGMC system

Evolution of segregation / partition coefficient with temperature

This is very interesting graph (Figure 8) which shows the relationship between temperature dependent partition coefficients as a function of increasing temperature itself. It shows that partition coefficient is not uniform in its behavior when studied over a temperature range. it evolves with the change / evolution of temperature. Although assumed to be and observed to be almost linear, its evolution is highly dependent on the gap which you will choose to calculate the values. The smaller the temperature gap, better will be the representation of actual behavior or evolution of partition coefficient over that period. For simplicity reasons, this effect is not studied in detail and general assumption that it shows linearity of evolution over temperature and time in the range of interest is made and adopted. Again thermal gradient is kept constant at 100 K / mm

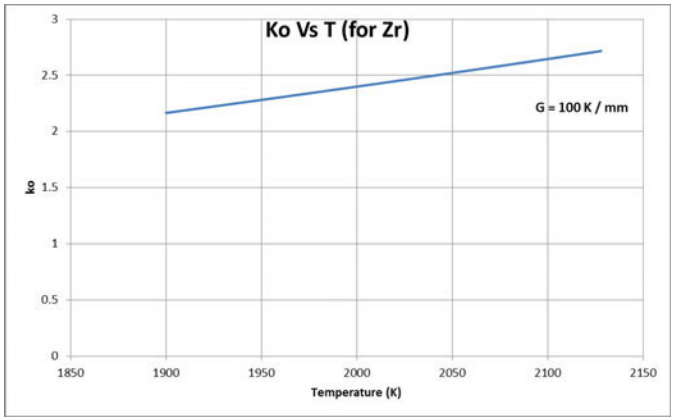

Figure 8: Plot of evolution of partition coefficient with temperature for Zr in BMGMC system at constant thermal gradient.

Effect of dendrite tip growth velocity on supersaturation

This is final and second most important graph (Figure 9) of this study. It describes the relationship of supersaturation for Zirconium only with dendrite tip growth velocity. This describes how a dendrite tip evolves and what happens to solute field around it as time passes and temperature decreases. As was expected and seen in experimental studies, it can be observed in this simulation as well that solute field around dendrite tip decreases almost in linear uniform homogenous fashion over a temperature range. This means that, solvent (alloy) keeps on rejecting solute as it solidifies and its dendritic structure evolves. This is also consistent with experimental observations made for a range of alloy systems previously [46, 59]. The drop in supersaturation is very sharp in first region as equiaxed grains are forming during this stage which are large in number and form very quickly followed by achievement of stability (a very small flat region in curve) because of equiaxed – columnar transition followed by almost linear

drop of slope of curve due to formation of columnar dendrites which are large in shape, move fast thus become source of large surface / volume ratio and faster rate of heat and mass transfer. Similar observations and simulation results are expected for other constituents provided temperature gradient is kept constant at 100 K / mm.

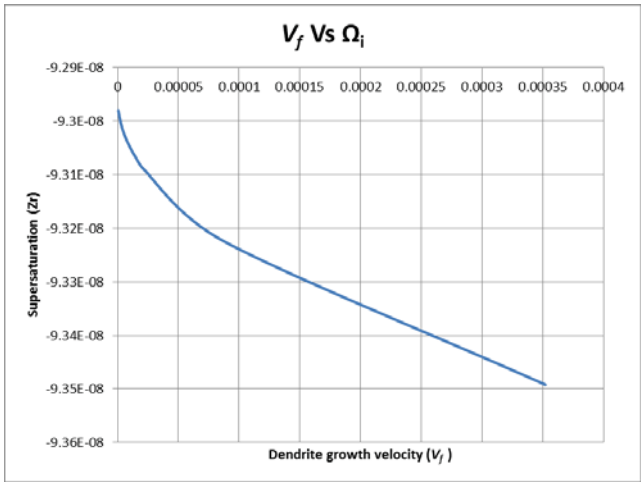

Figure 9: Plot of evolution of dendrite tip growth velocity as a function of supersaturation for Zr in BMGMC system at constant thermal gradient.

CONCLUSIONS

Following conclusions are drawn out of this study

(a) There is significant effect of initial metal temperature, composition, type of alloying elements, temperature gradient and thermo-physical properties on final microstrostructure developed as a result of heat and mass transfer phenomena.
(b) Determination of supersaturation of individual elements yields best possible strategy for its correlation with superimposition of solute field around each dendrite tip.
(c) Determination of dimensionless solutal Peclet number is the main factor responsible for accurate quantitative prediction of microstructure in solidifying alloys.
(d) Dependence and evolution of ξ on and with respect to solutal Peclet number is decisive in explaining transient nature transport phenomena in additive manufacturing processes.
(e) Employment of iterative process helps in refining the model and generates accurate results.

(f) Final microstructure evolution is expressed in the form of dendrite tip temperature and dendrite tip radius as a function of growth rate / dendrite tip velocity and must be carefully measured.

In essence, model comprises of extension of KGT theory for multicomponent systems beyond BLL model [61] employing real time temperature dependent conditions in Additive Manufacturing. All these considerations must be taken into account while designing an alloy system (present case BMGMC) for a practical application. Any fault or carelessness will result in erroneous reading and in worst case scenario, catastrophic failure of components, parts and assemblies which must be avoided.

ACKNOWLEDGMENTS

This work is supported by Dr. Dong Qiu's Vice Chancellor Senior Research Fellow Grant and Scholarship provided by RMIT University for tuition and living of author. Further, author would like to acknowledge moral support and encouragement provided by his primary supervisor (Dr. Dong Qiu) throughout the work and helpful discussion and constructive criticism by Prof. Mark Easton. The authorization of gracious use of experimental facilities during short term stay at CSIRO is also acknowledged.

REFERENCES

1. Klement, W., R.H. Willens, and P.O.L. Duwez, Nat, **187**(4740), 869-870 (1960)
2. Johnson, W.L., MRS Bull., **24**(10), 42-56 (1999)
3. Ashby, M.F. and A.L. Greer, Scr. Mater., **54**(3), 321-326 (2006)
4. Flores, K.M. and R.H. Dauskardt, J. Mater. Res. **14**(03), 638-643 (1999)
5. Eckert, J., et al., J. Mater. Res. **22**(02), 285-301 (2007)
6. Das, J., et al., J. Alloys Compd., **483**(1–2), 97-101 (2009)
7. Das, J., et al., Phys. Rev. Lett., **94**(20), 205501 (2005)
8. Choi-Yim, H. and W.L. Johnson, App. Phys. Lett., **71**(26), 3808-3810 (1997)
9. Cheng, J.L. and G. Chen, J Alloys Compd. **577,** 451-455 (2013)
10. Chen, M., NPG Asia Mater., **3,** 82-90 (2011)
11. Chen, M., Annu. Rev. Mater. Res., **38**(1) 445-469 (2008)
12. Chen, H.S., Acta Metall., **22**(12), 1505-1511 (1974)
13. Akihisa, I., et al., Jpn. J Appl. Phys., Part 1, **27**(9A), L1579 (1988)
14. Johnson, W.L., et al., Sci., **332**(6031), 828-833 (2011)
15. Jiang, M.Q., et al., Intermetallics, **18**(12), 2468-2471 (2010)
16. Qiao, J., H. Jia, and P.K. Liaw, Mater. Sci. Eng., R, **100,** 1-69 (2016)
17. Schroers, J., Adv. Mater. **22**(14), 1566-1597 (2010)
18. Greer, A.L., Nat., **464**(7292), 1137-1138 (2010)
19. Greer, A.L., Sci., **267**(5206), 1947-1953 (1995)
20. Yi, J., et al., Adv. Eng. Mater., **18**(6), 972-977 (2016)
21. Cheng, Y.Q., H.W. Sheng, and E. Ma, Phys. Rev. B, **78**(1), 014207 (2008)
22. Sarac, B., Springer, 2015
23. Greer, A.L., Nat Mater, **10**(2), 88-89 (2011)
24. Gu, X.W., et al., Nano Lett., **14**(10), 5858-5864 (2014)
25. Schroers, J. and W.L. Johnson, Phys. Rev. Lett., **93**(25), 255506 (2004)

26. Schuh, C.A., T.C. Hufnagel, and U. Ramamurty, Acta Mater., **55**(12), 4067-4109 (2007)
27. Donovan, P.E. and W.M. Stobbs, Acta Metall., **29**(8), 1419-1436 (1981)
28. Dodd, B. and Y. Bai, Elsevier, 2012
29. Gao, Y.F., et al., Acta Mater., **59**(10), 4159-4167 (2011)
30. Greer, A.L., Y.Q. Cheng, and E. Ma, Mater. Sci. Eng., R, **74**(4), 71-132 (2013)
31. Jiang, M.Q., W.H. Wang, and L.H. Dai, Scr. Mater., **60**(11), 1004-1007 (2009)
32. Leng, Y. and T.H. Courtney, J. Mater. Sci., **26**(3), 588-592 (1991)
33. Hajlaoui, K., et al., Mater. Sci. Eng., A, **449–451,** 105-110 (2007)
34. Lewandowski , J.J., W.H. Wang, and A.L. Greer, Philos. Mag. Lett, **85**(2), 77-87 (2005)
35. Zhang, Y. and A.L. Greer, J. of Alloys Compd., **434–435**, 2-5 (2007)
36. Zhang, T., et al., Metall. Mater. Trans. A, **45**(5), 2382-2388 (2014)
37. Liu, Y.H., et al., Sci., **315**(5817), 1385-1388 (2007)
38. Nishiyama, N., et al., Intermetallics, **30,** 19-24 (2012)
39. Schroers, J., JOM, **57**(5), 35-39 (2005)
40. Guo, G.-Q., et al., Metals, **5**(4), 2093 (2015)
41. Guo, G.-Q., et al., Metals, **5**(4), 2048 (2015)
42. Zu, F.-Q., Metals, **5**(1), 395 (2015)
43. Kim, D.H., et al., Prog. Mater. Sci., **58**(8), 1103-1172 (2013)
44. Ott, R.T., et al., Acta Mater., **53**(7), 1883-1893 (2005)
45. Rappaz, M. and C.A. Gandin, Acta Metall. Mater., **41**(2), 345-360 (1993)
46. Kurz, W., B. Giovanola, and R. Trivedi, Acta Metall., **34**(5), 823-830 (1986)
47. Wei, Y.H., et al., Sci. Technol. Weld. Joining, **12**(2), 138-146 (2007)
48. Rappaz, M. and E. Blank, J. Cryst. Growth, **74**(1), 67-76 (1986)
49. Rappaz, M., et al., Metall. Trans. A, **20**(6), 1125-1138 (1989)
50. Rappaz, M., et al., Metall. Trans. A, **21**(6), 1767-1782 (1990)
51. Gandin, C.-A., M. Rappaz, and R. Tintillier, Metall. Trans. A, **24**(2), 467-479 (1993)
52. Zhang, J., et al. In Proc. 24th. Int. Solid Freeform Fabr. Symp. UTexas Press, 739-48 (2014)
53. Zhou, X., et al., J. Mater. Sci., **51**(14), 6735-6749 (2016)
54. Gu, C., et al., Sci. and Technol. Weld. Joining, **22**(1), 47-58 (2017)
55. Nastac, L., Acta Mater., **47**(17), 4253-4262 (1999)
56. Laurentiu, N. and M.S. Doru, Modell. Simul. Mater. Sci. Eng., **5**(4), 391 (1997)
57. Von Neumann, J. and A.W. Burks, University of Illinois Press Urbana, 1996 (original 1950)
58. Reuther, K. and M. Rettenmayr, Comput. Mater. Sci., **95,** 213-220 (2014)
59. Mullins, W.W. and R.F. Sekerka, J App. Phys., **35**(2), 444-451 (1964)
60. Langer, J.S. and J. Müller-Krumbhaar,. J. Cryst. Growth, **42,** 11-14, (1977)
61. Bobadilla, M., J. Lacaze, and G. Lesoult, J. Cryst. Growth, **89**(4), 531-544 (1988)
62. Yang, G., et al., Intermetallics, **22,** 110-115 (2012)
63. *Mills, Kenneth C*, in *Recommended Values of Thermophysical Properties for Selected Commercial Alloys*. Woodhead Publishing (2002)
64. *GRIMVALL, GÖRAN*, in *Thermophysical Properties of Materials*. Elsevier Science B.V.: Amsterdam. (1999)
65. Valencia, J.J. and P. Quested, Model. Cast. Solidification Processing, 189 (2001)
66. Wu, K., R. Li, and T. Zhang, AIP Advances, **3**(11), 112115 (2013)
67. Yamasaki, M., S. Kagao, and Y. Kawamura, Scr. Mater., **53**(1), 63-67 (2005)

68. Choy, C.L., et al., J App. Phys., **70**(9), 4919-4925 (1991)